Evolution of the Bidirectional Vortex in a Capped Ellipsoidal Cyclonic Rocket Engine

Patrick Eid* and Joseph Majdalani†
Auburn University, Auburn, AL 36849

This work introduces an exact inviscid solution for the cyclonic motion that is engendered in a bidirectional vortex engine with a semi-elliptical chamber configuration. The swirling motion is initiated by a tangentially injected gaseous stream at the inner circumference of the chamber's equatorial plane. The ensuing helical updraft adheres to the chamber dome, reverses direction while curving around, and exits through the central core. The present analysis is based on the Bragg–Hawthorne equation, a compact streamfunction formulation that is well adapted to model steady, incompressible, and axisymmetric helical motions. By enforcing appropriate boundary conditions, an exact analytical solution is obtained for the Stokes streamfunction in both spherical and cylindrical coordinates. Being a parent function, the streamfunction enables us to derive closed-form expressions for most fundamental flow properties assuming both prolate and oblate ellipsoidal configurations. Owing to the intrinsic ellipsoidal curvature, the cyclonic stream also gives rise to a polar mantle across which the flow transitions to a purely radial inward motion. Along this lower ellipsoidal boundary, the polar velocity vanishes once while reversing its angular orientation. Unsurprisingly, both the polar and axial mantles merge in the exit plane, where the ideal outlet radius of the chamber can be deduced from this collocated position. The latter leads to an optimal exit diameter of approximately 70.7 percent of the capped-ellipsoidal chamber diameter. It thus reproduces the same mantle fraction associated with the analogous flowfield that arises in a right-cylindrical vortex chamber with a predominantly complex-lamellar motion.

I. Introduction

ROTATING flows are of tremendous interest to both natural and engineered systems given their ability to extend over an immense range of spatial and temporal scales. In geophysical and astrophysical applications, swirling motions may be associated with the evolution of tornadoes, dust devils, typhoons, hurricanes, tropical cyclones, planetary vortices, and even galactic pinwheels [1–4]. In biological systems, vortex-induced motions have been observed in the circulatory system, particularly in the aortic sinuses, where swirl facilitates blood flow regulation [5]. Technologically, the exploitation of vortex structures has led to numerous advancements in power and propulsion systems, where cyclonic flows have been leveraged to promote flame stabilization, enhanced mixing, improved heat transfer, and prolonged fuel residence times[6–8]. Industrial applications that rely on confined vortex flowfields include cyclone separators, vortex tubes, and gas turbine combustors, where swirl-induced separation, self-cooling effects, and compact volumetric designs provide distinct advantages [9–11].

In the propulsion community, bidirectional vortex combustors have emerged as a promising alternative to traditional rocket engine designs. These systems induce a cyclonic flowfield through wall-tangential injection. At the outset, they give rise to a characteristic bidirectional motion that consists of an outer, headwall-directed annular vortex and an inner, nozzle-directed core vortex. These flow regions remain separated by a virtual interface known as the *mantle*. The latter serves as a virtual transition layer in vortex-driven combustion chambers between the so-called updraft and downdraft. To date, several bidirectional vortex combustion devices have been developed, including the Vortex Combustion Ramjet [12], the Vortex Combustion Combined Cycle (VCCC) engine [13], and the Vortex Combustion Cold-Wall (VCCW) thrust chamber pictured in Fig. 1a [14, 15]. The potential benefits of these engines include prolonged residence times, improved flame stability, reduced wall heating, enhanced combustion efficiency, and greater equivalence ratio control. Such characteristics make them ideal candidates for hybrid and liquid rocket applications[16, 17]. The Vortex Injection Hybrid Rocket Engine (VIHRE)[18–20], shown in Fig. 1b, constitutes another such system; therein, a cyclonic flowfield is incorporated to enhance propellant regression and maximize performance in a hybrid propulsion setting.

So far, most theoretical and computational investigations of bidirectional vortex motion have focused on cylindrical and conical chambers. Computational studies have also relied on Reynolds-averaged Navier–Stokes (RANS) solvers, large eddy simulations (LES), and finite-element techniques [15, 21–25]. To a lesser degree, analytical models have been developed using, in large part, inviscid flow formulations and the Bragg–Hawthorne equation [26–30]. These

*Graduate Research Associate, Department of Aerospace Engineering. Member AIAA.
†Professor and Francis Chair, Department of Aerospace Engineering. Fellow AIAA.

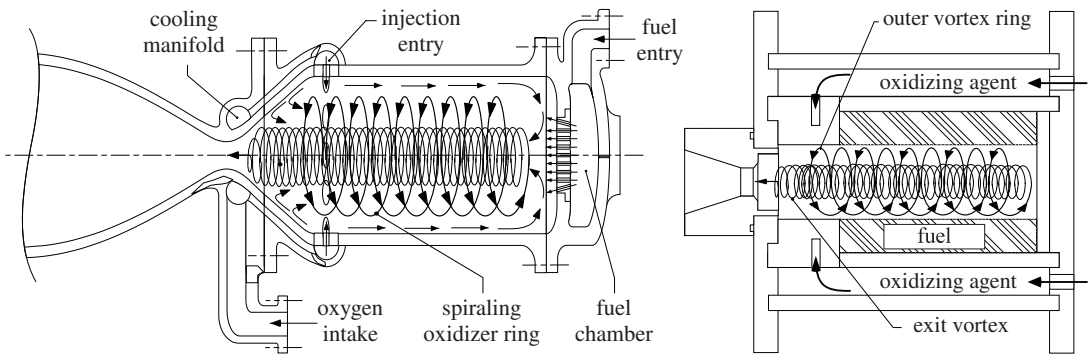

a) VCCW **b)** VIHRE

Fig. 1. Schematics of Sierra Space's a) Vortex Injection Hybrid Rocket Engine (VIHRE) conceived by Knuth et al. [18] and b) the Vortex Combustion Cold-Wall (VCCW) chamber developed by Chiaverini et al. [14].

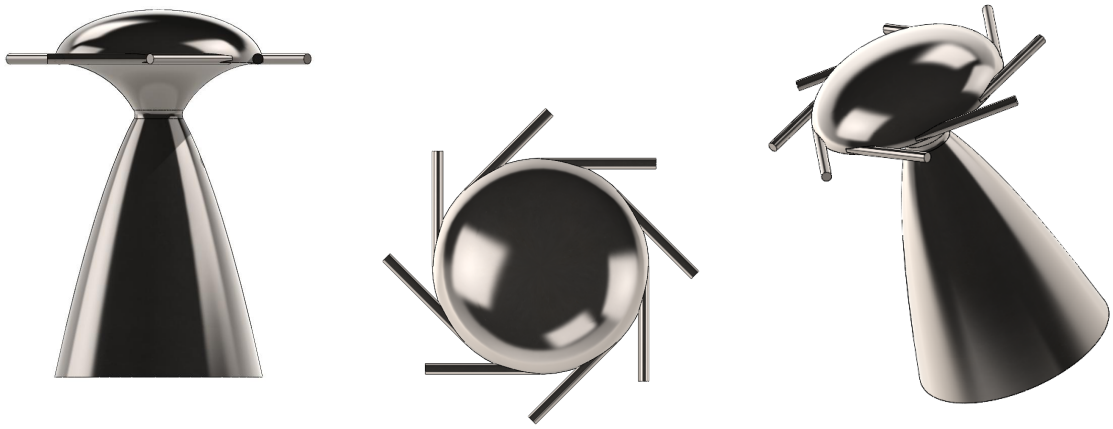

a) Side view **b)** Top view **c)** Isometric view

Fig. 2. Semi-ellipsoidal concept for compact, cyclonic rocket engines using a) side, b) top, and c) isometric views.

models have produced families of complex-lamellar, Beltramian, and Trkalian solutions that characterize the helical structure of cyclonic flowfields in right-cylindrical [31, 32, 35] and conical chambers [37–39]. Recent advancements have extended these analytical frameworks to spherical and hemispherical enclosures [40–42], thus leading to new classes of inviscid solutions that apply to rotationally axisymmetric geometries. However, the semi-ellipsoidal (or capped ellipsoidal) chamber configuration, which has been associated with advanced vortex engine concepts under development by Sierra Space Corporation, remains unexplored. Schematics of such a chamber are provided in Fig. 2.

The present work seeks to fill this gap by deriving an exact solution for the cyclonic motion evolving inside a capped ellipsoidal chamber. In comparison to cylindrical configurations, semi-ellipsoidal chambers provide higher volumetric efficiency, enhanced swirl-induced recirculation, and improved stability characteristics while maintaining a compact form factor. The derivation will be initiated from the axisymmetric Bragg–Hawthorne equation, where a transformed ellipsoidal coordinate representation will be pursued to extract closed-form approximations for the flow properties.

Despite the multitude of numerical investigations into confined cyclonic flows, analytical models that accurately predict vortex behavior in semi-ellipsoidal enclosures remain unavailable. Although former studies have demonstrated that vortex structures in right-cylindrical chambers exhibit predictable pressure and velocity profiles, the character of an ellipsoidal flow configuration warrants its own analysis. This work will therefore extend previous formulations of cyclonic motions by producing a formulation that accounts for the curvature effects of an ellipsoidal chamber. The

resulting incompressible and inviscid formulation will then serve as a fundamental benchmark for future analytical, computational, and experimental investigations. For example, it will form the basis for pursuing compressible and matched-asymptotic approximations that take into account both wall and core boundary layers.

The remainder of this article is organized as follows: First, the problem is formulated by specifying the governing equations, boundary conditions, and geometric details of a semi-ellipsoidal vortex chamber. Next, an exact analytical solution is derived using separation of variables, thus leading to closed-form expressions for the streamfunction, velocity components, vorticity, and pressure distribution. The findings are then compared to existing cyclonic models for wall-bounded cylindrical and hemispherical flows to the extent of showcasing the main advantages and limitations of an ellipsoidal chamber. Finally, the study concludes with several physical insights, potential applications, and recommendations for future work.

II. Problem Formulation and Solution Procedure

As shown in Fig. 3, we consider a semi-ellipsoidal domain that may be described in both spherical and cylindrical coordinates. The corresponding domain is bounded by $0 \le R \le a$, $0 \le \phi \le \pi/2$ and $0 \le \theta \le 2\pi$. In this idealization, the fluid is assumed to be frictionless. By further assuming steady, incompressible, and axisymmetric conditions with constant thermophysical properties, Euler's momentum equation reduces quite seamlessly to the Bragg–Hawthorne formulation. These assumptions not only simplify the governing equations but also facilitate the derivation of a closed-form analytical solution that captures the essential dynamics of the cyclonic flowfield. In fact, the use of an inviscid and incompressible motion is routinely used in the community. Culick [46], for example, employs nearly identical assumptions to obtain a mean flow approximation for internally-burning solid rocket motors. In what follows, a similar assortment of physical requirements will enable us to extract a fundamental approximation for the steady flow profile in the absence of chemical reactions.

A. Geometric Description

In the coordinate system shown in Fig. 3, the radial coordinate R extends outward from the origin of the semi-ellipsoidal domain. The polar angle ϕ and the azimuthal angle θ remain distinct, with θ maintaining its conventional definition in both coordinate systems. Under the assumption of axisymmetry, the streamfunction can be represented by $\psi(R, \phi)$ or, alternatively, $\psi(r, z)$.

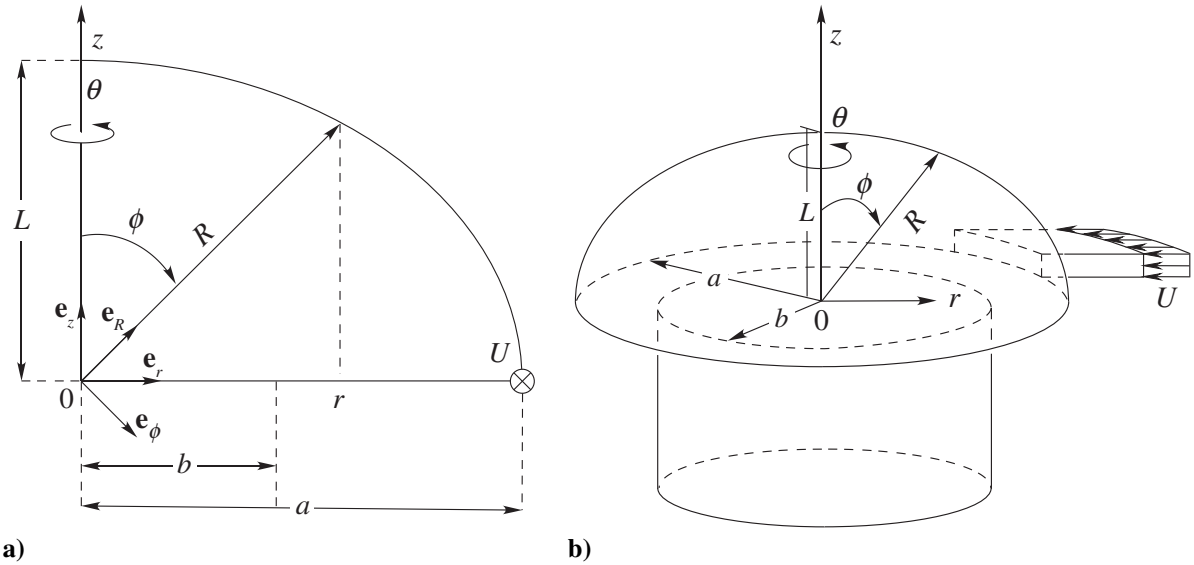

a) b)

Fig. 3. Solution domain depicting various spatial variables, polar and azimuthal angles, reference lengthscales, and unit vectors in both a) two-dimensional and b) three-dimensional views of a semi-ellipsoidal chamber.

B. Basic Assumptions and Governing Equation

We use the Bragg–Hawthorne equation (BHE) as our starting point, wherein the vorticity and velocity may be expressed in terms of the streamfunction. First presented in cylindrical coordinates by Bragg and Hawthorne [26], a spherical variant may be written as [42];

$$\frac{\partial^2\psi}{\partial R^2} + \frac{\sin\phi}{R^2}\frac{\partial}{\partial\phi}\left(\frac{1}{\sin\phi}\frac{\partial\psi}{\partial\phi}\right) = R^2\sin^2\phi\,\frac{\mathrm{d}H}{\mathrm{d}\psi} - B\,\frac{\mathrm{d}B}{\mathrm{d}\psi}. \tag{1}$$

In the above, $B(\psi)$ denotes the tangential angular momentum and H represents the stagnation pressure head. In Eq. (1), specifying B and H is essential. Since $H = H(\psi)$ according to Bernoulli's theorem, allowing a linear variation with ψ yields the lowest-order relation necessary for a closed-form rotational solution. Conversely, setting $H = 0$ leads to an irrotational profile, as shown by Williams and Majdalani [41]. Although nonlinear relations can be further explored [32], they fall beyond the scope of this study. In view of angular momentum conservation, one may assume a constant value of $B = ru_\theta$, as justified by the absence of frictional and heat losses [47, 48]. Eliminating the angular momentum gradient and setting $H = C^2\psi$, Eq. (1) reduces to

$$\frac{\partial^2\psi}{\partial R^2} + \frac{\sin\phi}{R^2}\frac{\partial}{\partial\phi}\left(\frac{1}{\sin\phi}\frac{\partial\psi}{\partial\phi}\right) = C^2R^2\sin^2\phi. \tag{2}$$

In cylindrical coordinates, Eq. (2) becomes

$$\frac{\partial^2\psi}{\partial r^2} - \frac{1}{r}\frac{\partial\psi}{\partial r} + \frac{\partial^2\psi}{\partial z^2} = C^2r^2. \tag{3}$$

C. Streamfunction Representation and Boundary Conditions

In cylindrical and spherical coordinates, the non-swirling velocity components can be expressed in terms of the Stokes streamfunction using

$$u_r = -\frac{1}{r}\frac{\partial\psi}{\partial z}, \quad u_z = \frac{1}{r}\frac{\partial\psi}{\partial r}, \quad u_R = \frac{1}{R^2\sin\phi}\frac{\partial\psi}{\partial\phi}, \quad \text{and} \quad u_\phi = -\frac{1}{R\sin\phi}\frac{\partial\psi}{\partial R}. \tag{4}$$

As for the problem's fundamental constraints, they arise from axisymmetry, confinement within the semi-ellipsoidal dome, and mass conservation. These physical requirements may be conveyed to the velocity components using:

$$u_\phi(0,\phi) = 0 \qquad \text{(no flow across the centerline)}, \tag{5}$$

$$u_R\left(\sqrt{a^2\cos^2\phi + L^2\sin^2\phi}, \phi\right) = 0 \qquad \text{(no flow across the wall)}, \tag{6}$$

$$2\pi\int_0^b u_z(r,0)r\,\mathrm{d}r = UA_i \qquad \text{(inflow-outflow mass balance)}, \tag{7}$$

$$u_\theta(a,\pi/2) = U \qquad \text{(specified average tangential speed at entry)}. \tag{8}$$

where U and A_i denote the average injection velocity and area, as shown in Fig. 3. Implicit in these assumptions is the rapid transition of the tangential inflow, UA_i, into axial motion at the base, with three-dimensional turning occurring near entry. Similar inlet flow turning assumptions in cyclonic chambers are made by Bloor and Ingham [37], Vyas and Majdalani [31], Alekseenko et al. [49], and Maicke and Talamantes [50]. After traversing the chamber and reversing its flow direction axially, the fluid exits through a circular outlet of radius b at $z = 0$.

D. Quasi Complex-Lamellar Solution

Using a streamfunction expression that is akin to that employed by Majdalani and Williams [40] for the treatment of hemispherically-bounded cyclones, we let

$$\psi(r,z) = \psi_0 r^2\left(1 - \frac{r^2}{a^2} - \frac{z^2}{L^2}\right), \tag{9}$$

where a and L denote the major and minor axes of our ellipsoidal chamber, as shown in Fig. 3. The leading coefficient ψ_0 may be deduced in this case from mass conservation in the equatorial plane. Forthwith, Eq. (7) yields

$$\psi_0 = -\frac{UA_i a^2}{2\pi b^2\left(a^2-b^2\right)}. \tag{10}$$

Naturally, backward substitution of ψ_0 into Eq. (9) enables us to fully determine the streamfunction as well as the radial and axial velocities. Additionally, by pairing our constant angular momentum expression for $B = ru_\theta$ with Eq. (8), u_θ may be immediately secured. In summary, we get

$$\begin{cases} \psi(r,z) = -\dfrac{UA_i a^2}{2\pi b^2(a^2-b^2)}\, r^2\left(1-\dfrac{r^2}{a^2}-\dfrac{z^2}{L^2}\right), \\ u_r(r,z) = -\dfrac{UA_i a^2}{\pi b^2(a^2-b^2)}\dfrac{rz}{L^2}, \\ u_z(r,z) = -\dfrac{UA_i a^2}{\pi b^2(a^2-b^2)}\left(1-\dfrac{2r^2}{a^2}-\dfrac{z^2}{L^2}\right), \\ u_\theta(r) = \dfrac{Ua}{r}. \end{cases} \tag{11}$$

Along similar lines, two geometric transformations of the form of $u_R = u_r \sin\phi + u_z \cos\phi$ and $u_\phi = u_z \sin\phi - u_r \cos\phi$ may be used to retrieve the spherical components, specifically:

$$\begin{cases} u_R(R,\phi) = -\dfrac{UA_i a^2}{\pi b^2\left(a^2-b^2\right)}\cos\phi\left[1-R^2\left(\dfrac{2\sin^2\phi}{a^2}+\dfrac{\cos^2\phi-\sin^2\phi}{L^2}\right)\right], \\ u_\phi(R,\phi) = \dfrac{UA_i a^2}{\pi b^2\left(a^2-b^2\right)}\sin\phi\left[1-2R^2\left(\dfrac{\sin^2\phi}{a^2}+\dfrac{\cos^2\phi}{L^2}\right)\right], \\ u_\theta(R,\phi) = \dfrac{Ua}{R\sin\phi}. \end{cases} \tag{12}$$

These may be complemented by the cylindrical radial and axial velocities in terms of spherical coordinates:

$$\begin{cases} u_r(R,\phi) = -\dfrac{UA_i a^2}{2\pi b^2\left(a^2-b^2\right)}\dfrac{R^2\sin(2\phi)}{L^2}, \\ u_z(R,\phi) = -\dfrac{UA_i a^2}{\pi b^2\left(a^2-b^2\right)}\left[1-R^2\left(\dfrac{2\sin^2\phi}{a^2}+\dfrac{\cos^2\phi}{L^2}\right)\right]. \end{cases} \tag{13}$$

The solution for a wall-bounded semi-ellipsoidal cyclone and its various components is therefore at hand. Note that the singularity plaguing u_θ as $r \to 0$ constitutes an expected and well-documented outcome of angular momentum conservation [47, 48]. In fact, it may be gratifying to verify that the resulting profile satisfies Eq. (3) identically along with all boundary conditions given by Eqs. (5–8). It therefore represents an exact solution to Euler's equation. Furthermore, by limiting ourselves to the r-z plane, it may be shown that the inner product of the velocity and vorticity vectors vanishes. This may be accomplished by ignoring the irrotational vortex contribution of the decoupled velocity, u_θ. Since any velocity field $\boldsymbol{u}$ satisfying $\boldsymbol{u}\cdot(\nabla\times\boldsymbol{u}) = 0$ is termed "complex lamellar," the present solution may be regarded as being "quasi complex lamellar." At first glance, it may be seen to exhibit similar characteristics to its helical flow counterparts in cylindrical [31] and hemispherical chambers [40].

III. Results and Discussion

With the availability of an exact solution, its fundamental characteristics can be carefully examined. In view of the semi-ellipsoidal curvature at play, two distinct mantles can be identified that divide the flow domain slightly differently. These will be referred to as the axial and polar mantles, as they also arise in hemispherically-bounded cyclonic flowfields [40–42].

A. Axial Mantle Analysis

The axial mantle is defined as the rotating non-translating interfacial layer along which the axial velocity vanishes. By imposing $u_z = 0$, the vertical axis projections of the polar and radial velocities become equivalent. One gets:

$$-\frac{UA_i a^2}{\pi b^2(a^2-b^2)}\left(1-\frac{2r^2}{a^2}-\frac{z^2}{L^2}\right)=0. \tag{14}$$

The resulting expression yields a relation for the axial mantle as a function of r, a, and L. Using an asterisk to denote the spatial locus of the mantle surface, z^*_{axial}, one can put

$$z^*_{\text{axial}} = L\sqrt{1-\frac{2r^2}{a^2}}, \quad 0 \le r \le \frac{a}{\sqrt{2}}, \tag{15}$$

where z^*_{axial} emerges as a function of three distinct parameters, unlike its counterparts in cylindrical and conical geometries [31, 37, 38, 51]. We may also determine the corresponding locus in spherical coordinates as well as the radial crossflow velocity, which is responsible for mass transport from the so-called updraft (or outer vortex) to the downdraft (or inner vortex). We obtain,

$$R^*_{\text{axial}} = \frac{aL}{\sqrt{2L^2\sin^2\phi + a^2\cos^2\phi}} \quad \text{and} \quad (u_r)_{\text{cross}} = \frac{\psi_0 R^{*2}_{\text{axial}}\sin(2\phi)}{L^2} = \frac{a^2\psi_0\sin(2\phi)}{2L^2\sin^2\phi + a^2\cos^2\phi}. \tag{16}$$

Equation (16) defines the axial mantle as a quadratic surface that forms half of a prolate spheroid, with the particular semi-axes of $(a/\sqrt{2}, a/\sqrt{2}, L)$. Unsurprisingly, when the axial mantle is positioned in the exit plane, where $\phi = \pi/2$, its intersection with the equatorial plane returns the corresponding mantle of a right-cylindrical cyclonic chamber. More specifically, one obtains a horizontal radius of $R^*_{\text{axial}}(\pi/2) = a/\sqrt{2}$, a value that coincides with the experimental findings of Smith [51] as well as those predicted using analytical models [31, 40]. Subsequently, by equating the domain's outlet radius to $b \approx 0.707a$, the outflow opening will precisely match the mantle's and, as such, promote a smooth outgoing motion that precludes wall collisions.

B. Polar Mantle Analysis

The polar mantle corresponds to the swirling interfacial layer where the polar velocity vanishes. By setting $u_\phi = 0$, the crossflow between the outer and inner regions becomes strictly radial inward. By imposing this condition in Eq. (12), we retrieve

$$R^*_{\text{polar}} = \frac{aL}{\sqrt{2\left(L^2\sin^2\phi + a^2\cos^2\phi\right)}} \quad \text{and} \quad (u_R)_{\text{cross}} = \psi_0\cos\phi\left[\frac{a^2}{L^2\sin^2\phi + a^2\cos^2\phi}\right]. \tag{17}$$

Unlike the axial mantle in a cylindrical chamber, where the crossflow velocity remains uniform, the radial inward velocity responsible for mass transport across the polar mantle, $(u_R)_{\text{cross}}$, varies spatially. As expected, it vanishes at $\phi = \pi/2$ and gradually increases in magnitude as it nears the centerline, reaching its maximum as $\phi \to 0$.

C. Flow Normalization

For further clarity and broader portability, it proves advantageous to normalize all variables and parameters of interest using, for the most part, the major axis, a, and the tangential injection speed, U. In this process, the modified swirl number, $\sigma \equiv A_i/a^2$, is defined [31, 50]. This parameter enables us to model the addition of identical injectors by simply accounting for the total increase in the overall inlet area, A_i. Moreover, a normalized exit radius, $\beta \equiv b/a$, can be introduced as the radial fraction of the outflow in the equatorial plane. To proceed, all non-dimensional variables are tagged with overbars and written as:

$$\begin{cases} \bar{r} = \dfrac{r}{a}, \quad \overline{R} = \dfrac{R}{a}, \quad \bar{z} = \dfrac{z}{a}, \quad \beta = \dfrac{b}{a}, \quad l = \dfrac{L}{a}, \quad \kappa = \dfrac{1}{2\pi\sigma l}, \quad \overline{\psi} = \dfrac{\psi}{Ua^2}, \quad \overline{H} = \dfrac{H}{U^2}, \quad \overline{B} = \dfrac{B}{aU}, \quad \overline{p} = \dfrac{p}{\rho U^2} \\ \bar{u}_r = \dfrac{u_r}{U}, \quad \bar{u}_R = \dfrac{u_R}{U}, \quad \bar{u}_\phi = \dfrac{u_\phi}{U}, \quad \text{and} \quad \bar{u}_\theta = \dfrac{u_\theta}{U}. \end{cases} \tag{18}$$

In the above, the inflow parameter κ appears to be inversely proportional to the swirl number. Using $\tilde{\kappa} \equiv \kappa/(\beta^2 - \beta^4)$, the non-dimensional form of the streamfunction becomes

$$\frac{\psi(R,\phi)}{Ua^2} = -\frac{l\kappa R^2 \sin^2\phi}{a^2\left(\beta^2-\beta^4\right)}\left(1 - \frac{R^2\sin^2\phi}{a^2} - \frac{R^2\cos^2\phi}{L^2}\right) \quad \text{or} \quad \bar{\psi} = l\,\tilde{\kappa}\,\bar{R}^2\sin^2\phi\left(\bar{R}^2\sin^2\phi + \frac{\bar{R}^2\cos^2\phi}{l^2} - 1\right). \tag{19}$$

In like fashion, the spherical velocity components collapse into:

$$\bar{u}_R = -2l\tilde{\kappa}\cos\phi\left[1 - \bar{R}^2\left(2\sin^2\phi + \frac{\cos^2\phi - \sin^2\phi}{l^2}\right)\right], \quad \bar{u}_\phi = 2l\tilde{\kappa}\sin\phi\left[1 - 2\bar{R}^2\left(\sin^2\phi + \frac{\cos^2\phi}{l^2}\right)\right], \tag{20}$$

with their cylindrical counterparts turning into,

$$\bar{u}_r = -\tilde{\kappa}\,\frac{\bar{R}^2}{l^2}\,\sin(2\phi), \quad \bar{u}_\theta = \frac{1}{\bar{R}\sin\phi}, \quad \text{and} \quad \bar{u}_z = -2\tilde{\kappa}\left[\frac{l^2 - 2l^2\bar{R}^2\sin^2\phi - \bar{R}^2\cos^2\phi}{l}\right]. \tag{21}$$

Lastly, the axial and polar crossflow velocities along with their mantle interfaces reduce to:

$$\begin{cases} (\bar{u}_r)_{\text{cross}} = \dfrac{-l\tilde{\kappa}\sin(2\phi)}{2l^2\sin^2\phi + \cos^2\phi} & \bar{R}^*_{\text{axial}} = l(2l^2\sin^2\phi + \cos^2\phi)^{-1/2} \\ (\bar{u}_R)_{\text{cross}} = -l\tilde{\kappa}\cos\phi\left[\frac{1}{l^2\sin^2\phi + \cos^2\phi}\right] & \bar{R}^*_{\text{polar}} = l(2l^2\sin^2\phi + 2\cos^2\phi)^{-1/2}. \end{cases} \tag{22}$$

D. Flow Topology

By taking into account the particular outlet fraction of $\beta = 1/\sqrt{2}$, one finds $\beta^2(1-\beta^2) = 1/4$; this produces $\tilde{\kappa} = 4\kappa$ from Eq. (20). The ideal, self-consistent profile with an outlet fraction matching the mantle radius becomes

$$\bar{\psi} = 4l\kappa\bar{R}^2\sin^2\phi\left(\bar{R}^2\sin^2\phi + \frac{\bar{R}^2\cos^2\phi}{l^2} - 1\right) = 4l\kappa\bar{r}^2\left(\bar{r}^2 + \frac{\bar{z}^2}{l^2} - 1\right). \tag{23}$$

As for the spherical velocities, they simplify into

$$\begin{cases} \bar{u}_R = -8l\kappa\cos\phi\left[1 - \bar{R}^2\left(2\sin^2\phi + \frac{\cos^2\phi - \sin^2\phi}{l^2}\right)\right] = -8\kappa\bar{z}(l^2 - 2\bar{r}^2l^2 - \bar{z}^2 + \bar{r}^2)/l\sqrt{\bar{r}^2 + \bar{z}^2} & \text{(spherical radial)}, \\ \bar{u}_\phi = 8l\kappa\sin\phi\left[1 - 2\bar{R}^2\left(\sin^2\phi + \frac{\cos^2\phi}{l^2}\right)\right] = 8\kappa\bar{r}(l^2 - 2l^2\bar{r}^2 - 2\bar{z}^2)/l\sqrt{\bar{r}^2 + \bar{z}^2} & \text{(polar)}, \\ \bar{u}_\theta = (\bar{R}\sin\phi)^{-1} = \bar{r}^{-1} & \text{(tangential)}. \end{cases} \tag{24}$$

Their strictly cylindrical components also collapse into

$$\begin{cases} \bar{u}_r = -8\kappa\bar{R}^2\sin\phi\cos\phi/l^2 = -8\kappa\bar{r}\bar{z}/l^2 & \text{(horizontal or radial)}, \\ \bar{u}_z = -8\kappa[1 - \bar{R}^2(1 + \sin^2\phi)] = -8\kappa(l^2 - 2l^2\bar{r}^2 - \bar{z}^2)/l & \text{(vertical or axial)}. \end{cases} \tag{25}$$

Finally, the compacted axial and polar mantle expressions return,

$$\bar{z}^*_{\text{axial}} = l\sqrt{1 - 2\bar{r}^2} \quad \text{and} \quad \bar{z}^*_{\text{polar}} = \sqrt{\tfrac{1}{2} - \bar{r}^2}, \tag{26}$$

where $\bar{r} \in [0, 1/\sqrt{2}]$.

E. Streamlines and Mantle Distributions

In the interest of clarity, vector plots of the streamfunction from Eqs. (23–25) are presented in Fig. 4 using $l = 0.6$ and 0.8 for an oblate ellipsoidal chamber, and in Fig. 5 using $l = 1.2$ and 1.4 for a prolate configuration. Although not shown, setting $l = 1$ enables us to recover all the results obtained for the hemispherically-bounded cyclonic motion

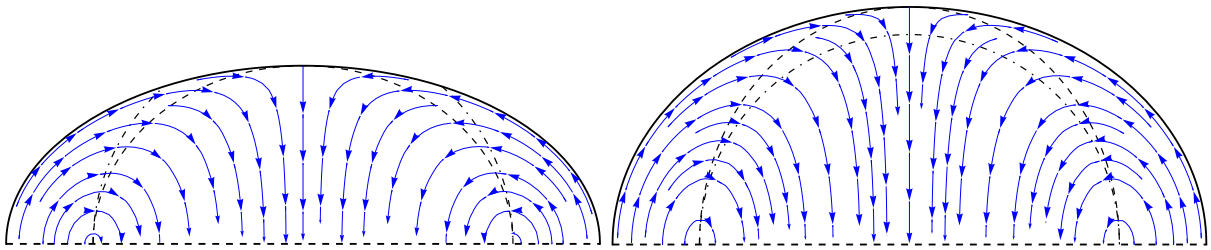

a) $l = 0.6$ **b)** $l = 0.8$

Fig. 4. Streamlines of a capped ellipsoidal oblate chamber taken in the r-z plane with an L value of a) $0.6a$ and b) $0.8a$, with both axial and polar mantles displayed. The latter refer to the $u_z = 0$ (– – –) and $u_\phi = 0$ (— · —) mantle distributions given by $\bar{z}^*_{\text{axial}} = l\sqrt{1-2\bar{r}^2}$ and $\bar{z}^*_{\text{polar}} = \sqrt{1/2-\bar{r}^2}$, respectively. Here $\kappa = 0.05$ and, unless specified differently, we take $\beta = 1/\sqrt{2}$ everywhere.

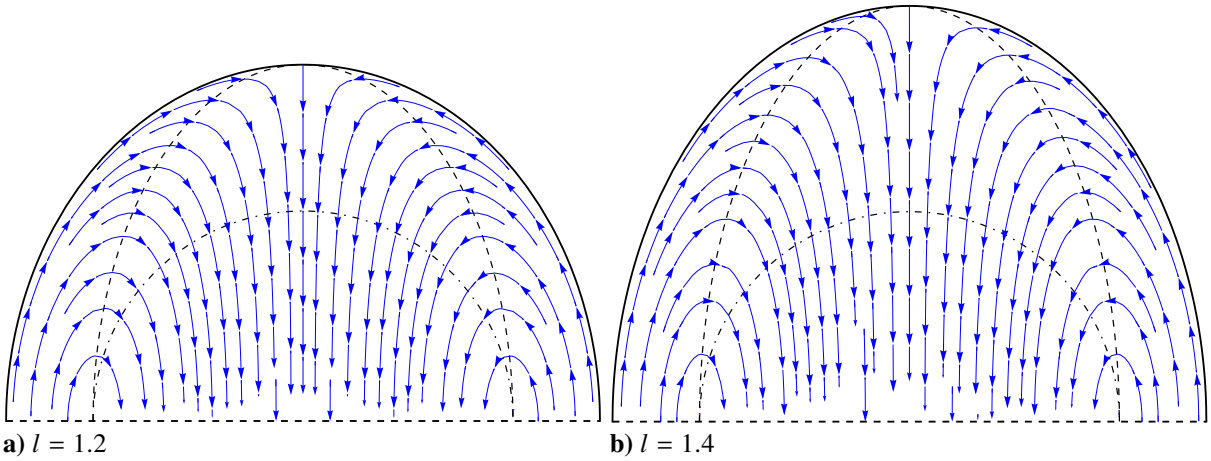

a) $l = 1.2$ **b)** $l = 1.4$

Fig. 5. Streamlines of a capped ellipsoidal prolate chamber taken in the r-z plane with an L value of a) $1.2a$ and b) $1.4a$, with both axial and polar mantles displayed. The latter refer to the $u_z = 0$ (– – –) and $u_\phi = 0$ (— · —) mantle distributions given by $\bar{z}^*_{\text{axial}} = l\sqrt{1-2\bar{r}^2}$ and $\bar{z}^*_{\text{polar}} = \sqrt{1/2-\bar{r}^2}$, respectively. Here $\kappa = 0.05$ and, unless specified differently, we take $\beta = 1/\sqrt{2}$ everywhere.

described by Majdalani and Williams [40]. Note that the broken and chained lines are used to depict the axial and polar mantles in all cases considered and for $\phi \in [0, \pi/2]$.

Using an illustrative value of $\kappa = 0.05$, the bidirectional nature of the helical motion is evident. The incoming fluid ascends along the chamber's curved semi-ellipsoidal wall, bends near the headend, reverses axial direction, and returns through the central inner flow region. Interestingly, the broken lines depicting the axial mantle fall below the chained polar mantle lines so long as $l \leq 0.707$. Otherwise, it envaginates the polar mantle as shown for $l = 0.8, 1.2$, and 1.4 in Figs. 4b, 5a and 5b.

In examining how the collocated mantles partition the flow domain, one may observe that the outer annular region, situated outside the broken line demarcating the axial mantle, exhibits positive (upward) axial velocities, whereas the inner core, lying below the elliptical boundary, is characterized by negative (downward) axial velocities. Meanwhile, the chained arc identifying the polar mantle divides the domain into a relatively broad annulus of nearly uniform radial thickness and a more compact inner region possessing outward-pointing polar velocities. Interestingly, the polar mantle's annulus extends deeper toward the centerline compared with its axial counterpart, which tapers off at a higher radial fraction. Consequently, a volumetric analysis reveals that the outer region defined by the polar mantle encompasses a larger fraction of the chamber volume than the inner region. Conversely, the subdivision caused by the axial mantle leads to an even partitioning of the domain, as it is formed by revolving an elliptical contour around the polar axis. This process yields two volumes of equal size, with the inner portion forming a prolate-like body of revolution.

Further inspection of the interfacial areas shows that the polar mantle surface remains both smaller and lower in elevation than its axial counterpart. As such, the polar interface presents a reduced crossflow area through which the fluid must migrate inwardly, being located at a lower position in the chamber. By comparing the vertical extents of the two outflow regions, one finds that the polar outflow zone lies at a lower centroidal height than its axial counterpart. From an application standpoint, lowering and shrinking the polar mantle can help mitigate early leakage of incoming oxidizer agents, thus promoting better mixing and reactions in the upper section of the semi-ellipsoidal chamber. Such an advantage has been recognized in designs that are aiming to limit premature radial infiltration and short-circuiting of freshly injected oxidizer streams [14, 52].

IV. Conclusions

This study presents an exact Eulerian solution describing the bidirectional cyclonic motion that develops within a capped-ellipsoidal vortex chamber, a configuration inspired by recent advances in vortex propulsion systems. By leveraging the Bragg–Hawthorne equation, the fundamental flow characteristics are captured in both spherical and cylindrical coordinates, thereby extending the existing body of analytical solutions for swirling motions in confined geometries.

Several key observations can be drawn from this analysis:

(i) Similarity of Streamlines: The streamfunction-based solution accurately reproduces the fluid trajectories of the evolving helical flowfield. The resulting velocity distributions are strongly dependent on the inflow parameter κ; the latter scales inversely with the modified swirl number, σ, thus reflecting the strong dependence of cyclonic flows on injection conditions.

(ii) Quasi Complex-Lamellar Motion: By neglecting the tangential component, the remaining velocity field exhibits properties associated with complex-lamellar flows, albeit in a quasi sense.

(iii) Identification of Dual Mantle Structures: Firstly, the axial mantle emerges as a non-translating interface where the axial velocity vanishes. Unlike its counterpart in cylindrical geometries, the axial mantle in an ellipsoidal chamber follows an elliptical profile, effectively partitioning the domain into an outer updraft annulus and an inner prolate-like downdraft region. The latter is centrally located and experiences a peak axial velocity at the centerline, though the tangential velocity continues to intensify as the core is approached. Secondly, the polar mantle, which is unique to hemispherical and semi-ellipsoidal enclosures, serves as a transition layer where the polar velocity vanishes. This region defines the interface between the outer and inner vortical regions exchanging mass across the chamber. The lower placement and reduced crossflow area of the polar mantle compared to cylindrical chambers minimizes early oxidizer leakage, an effect that is highly beneficial to propulsive efficiency in practical applications.

(iv) Outlet Optimization and Flow Partitioning: The intersection of axial and polar mantles in the exit plane occurs at a normalized radius that is consistent with findings related to right-cylindrical vortex chambers. By aligning the chamber's outlet radius with this mantle fraction, an unobstructed and self-consistent outflow condition is realized. This minimizes flow separation and backflow instabilities, thus leading to an idealized flow configuration.

(v) Geometric Advantages of the Ellipsoidal Configuration: The adoption of a semi-ellipsoidal chamber, rather than a cylindrical or conical one, leads to a reduced surface-to-volume ratio, inherently lowering wall heating rates and thermal losses. Additionally, its compact volumetric efficiency supports enhanced swirl-induced recirculation, thus offering improved stability characteristics. These features make the ellipsoidal bidirectional vortex engine particularly attractive for high-performance propulsion systems, where weight reduction translates directly into enhanced payload capacity and mission flexibility.

Overall, this study extends the analytical foundation of vortex combustion modeling by introducing a fully resolved inviscid solution that is tailored for capped ellipsoidal chambers. The findings serve as a benchmark for future computational and experimental studies aiming to explore viscous effects, compressibility corrections, and chemical reactions in next-generation swirl-assisted propulsion systems.

References

[1] Lugt, H. J., "Vortex Breakdown in Atmospheric Columnar Vortices," *Bulletin of the American Meteorological Society*, Vol. 70, No. 12, 1989, pp. 1526–1537. doi:10.1175/1520-0477(1989)070<1526:VBIACV>2.0.CO;2.

[2] Lee, S.-L., "Axisymmetrical Turbulent Swirling Natural-Convection Plume: Part 1—Theoretical Investigation," *Journal of Applied Mechanics*, Vol. 33, No. 3, 1966, pp. 647–655. doi:10.1115/1.3625134.

[3] Lee, S.-L., "Axisymmetrical Turbulent Swirling Natural-Convection Plume: Part 2—Experimental Investigation," *Journal of Applied Mechanics*, Vol. 33, No. 3, 1966, pp. 656–661. doi:10.1115/1.3625135.

[4] Fitzjarrald, D. E., "A Laboratory Simulation of Convective Vortices," *Journal of the Atmospheric Sciences*, Vol. 30, No. 5, 1973, pp. 894–902. doi:10.1175/1520-0469(1973)030<0894:ALSOCV>2.0.CO;2.

[5] Bellhouse, B. J. and Talbot, L., "The Fluid Mechanics of the Aortic Valve," *Journal of Fluid Mechanics*, Vol. 35, No. 4, 1969, pp. 721–735. doi:10.1017/S0022112069001406.

[6] Ribeiro, M. M. and Whitelaw, J. H., "Coaxial Jets with and without Swirl," *Journal of Fluid Mechanics*, Vol. 96, No. 04, February 1980, pp. 769. doi:10.1017/s0022112080002352.

[7] Park, S. H. and Shin, H. D., "Measurements of Entrainment Characteristics of Swirling Jets," *International Journal of Heat and Mass Transfer*, Vol. 36, No. 16, November 1993, pp. 4009–4018. doi:10.1016/0017-9310(93)90151-u.

[8] Örlü, R. and Alfredsson, P. H., "An Experimental Study of the Near-Field Mixing Characteristics of a Swirling Jet," *Flow, Turbulence and Combustion*, Vol. 80, No. 3, December 2007, pp. 323–350. doi:10.1007/s10494-007-9126-y.

[9] Hilsch, R., "The Use of the Expansion of Gases in a Centrifugal Field as Cooling Process," *Review of Scientific Instruments*, Vol. 18, No. 2, February 1947, pp. 108–113. doi:10.1063/1.1740893.

[10] Crocker, A. M., Sutphin, G. L., and Cassisi, D. V., "Investigation of Enhanced Vortex Tube Air Separators for Advanced Space Transportation," *40th AIAA/ASME/SAE/ASEE Joint Propulsion Conference and Exhibit*, AIAA Paper 2004-3392, June 2004. doi:10.2514/6.2004-3392.

[11] Sharma, G., Ghosh, S., and Karmakar, S., "Computational Fluid Dynamic Simulation of Single and Two-Phase Vortex Flow—A Comparison of Flow Field and Energy Separation," *Journal of Heat Transfer*, Vol. 138, No. 8, May 2016, pp. 082003. doi:10.1115/1.4033388.

[12] Knuth, W. H., Chiaverini, M. J., Gramer, D. J., and Sauer, J. A., "Final Report on Vortex Combustion Ramjet – A Phase I SBIR Project," SBIR Phase I, NASA Final Technical Contract No. NAS3-99039, OTC-GS075-FR-99-1, Madison, Wisconsin, June 1999.

[13] Chiaverini, M. J., Sauer, J. A., and Knuth, W. H., "Final Report on Vortex Combustion Combined Cycle Engine – A Phase I SBIR Project," AFRL Contract No. F04611-99-C-0063, OTC-GS082-FR-99-1, Madison, Wisconsin, March 1999.

[14] Chiaverini, M. J., Malecki, M., Sauer, J. A., Knuth, W. H., and Majdalani, J., "Vortex Thrust Chamber Testing and Analysis for O2-H2 Propulsion Applications," *39th AIAA/ASME/SAE/ASEE Joint Propulsion Conference and Exhibit*, AIAA Paper 2003-4473, July 2003. doi:10.2514/6.2003-4473.

[15] Majdalani, J. and Chiaverini, M. J., "Characterization of GO2–GH2 Simulations of a Miniature Vortex Combustion Cold-Wall Chamber," *Journal of Propulsion and Power*, Vol. 33, No. 2, March 2017, pp. 387–397. doi:10.2514/1.b36277.

[16] Chiaverini, M. J., Malecki, M., Sauer, J. A., Knuth, W. H., and Hall, C. D., "Vortex Combustion Chamber Development for Future Liquid Rocket Engine Applications," *38th AIAA/ASME/SAE/ASEE Joint Propulsion Conference and Exhibit*, AIAA Paper 2002-4149, July 2002. doi:10.2514/6.2002-4149.

[17] Majdalani, J., "Exact Eulerian Solutions of the Cylindrical Bidirectional Vortex," *45th AIAA/ASME/SAE/ASEE Joint Propulsion Conference and Exhibit*, AIAA Paper 2009-5307, August 2009. doi:10.2514/6.2009-5307.

[18] Knuth, W. H., Bemowski, P. A., Gramer, D. J., Majdalani, J., and Rothbauer, W. J., "Gas-Fed, Vortex Injection Hybrid Rocket Engine," SBIR Phase I, NASA Final Technical Contract No. NAS8-40679, Madison, Wisconsin, August 1996.

[19] Knuth, W. H., Chiaverini, M. J., Sauer, J. A., and Gramer, D. J., "Solid-Fuel Regression Rate Behavior of Vortex Hybrid Rocket Engines," *Journal of Propulsion and Power*, Vol. 18, No. 3, May 2002, pp. 600–609. doi:10.2514/2.5974.

[20] Chiaverini, M. J. and Kuo, K. K., editors, *Fundamentals of Hybrid Rocket Combustion and Propulsion*, Vol. 218, American Institute of Aeronautics and Astronautics, Reston, VA, 2007.

[21] Hsieh, K. T. and Rajamani, R. K., "Mathematical Model of the Hydrocyclone Based on Physics of Fluid Flow," *AIChE Journal*, Vol. 37, No. 5, May 1991, pp. 735–746. doi:10.1002/aic.690370511.

[22] Ogawa, A., *Vortex Flow*, CRC Press, Boca Raton, Fla, 1993.

[23] Hoekstra, A. J., van Vliet, E., Derksen, J. J., and van den Akker, H. E. A., "Vortex Core Precession in a Gas Cyclone," *Fluid Mechanics and Its Applications*. Springer Netherlands, 1998, pp. 289–292. doi:10.1007/978-94-011-5118-4_71.

[24] Derksen, J. J. and van den Akker, H. E. A., "Simulation of Vortex Core Precession in a Reverse-Flow Cyclone," *AIChE Journal*, Vol. 46, No. 7, July 2000, pp. 1317–1331. doi:10.1002/aic.690460706.

[25] Zhu, Z., Na, Y., and Lu, Q., "Pressure Drop in Cyclone Separator at High Pressure," *Journal of Thermal Science*, Vol. 17, No. 3, September 2008, pp. 275–280. doi:10.1007/s11630-008-0275-7.

[26] Bragg, S. L. and Hawthorne, W. R., "Some Exact Solutions of the Flow Through Annular Cascade Actuator Discs," *Journal of the Aeronautical Sciences*, Vol. 17, No. 4, April 1950, pp. 243–249. doi:10.2514/8.1597.

[27] Hicks, W. M., "Researches in Vortex Motion. Part III. On Spiral or Gyrostatic Vortex Aggregates," *Proceedings of the Royal Society of London*, Vol. 62, No. 379–387, January 1898, pp. 332–338. doi:10.1098/rspl.1897.0119.

[28] Long, R. R., "Steady Motion Around a Symmetrical Obstacle Moving Along the Axis of a Rotating Liquid," *Journal of Atmospheric Sciences*, Vol. 10, No. 3, 1953, pp. 197–203. doi:10.1175/1520-0469(1953)010<0197:SMAASO>2.0.CO;2.

[29] Squire, H. B., *Rotating Fluids*, Monographs on Mechanics and Applied Mathematics. Cambridge University Press, New York, 1956, pp. 139–161.

[30] White, F. M. and Majdalani, J., *Viscous Fluid Flow*, McGraw-Hill, New York, 4th ed., 2021.

[31] Vyas, A. B. and Majdalani, J., "Exact Solution of the Bidirectional Vortex," *AIAA Journal*, Vol. 44, No. 10, October 2006, pp. 2208–2216. doi:10.2514/1.14872.

[32] Majdalani, J. and Rienstra, S. W., "On the Bidirectional Vortex and Other Similarity Solutions in Spherical Coordinates," *Zeitschrift für angewandte Mathematik und Physik*, Vol. 58, No. 2, February 2007, pp. 289–308. doi:10.1007/s00033-006-5058-y.

[33] Akiki, G. and Majdalani, J., "On the Bidirectional Vortex with Arbitrary Endwall Velocity," *46th AIAA/ASME/SAE/ASEE Joint Propulsion Conference and Exhibit*, AIAA Paper 2010-6652, July 2010. doi:10.2514/6.2010-6652.

[34] Akiki, G., *On the Bidirectional Vortex Engine Flowfield with Arbitrary Endwall Injection*, Masters thesis, University of Tennessee, Knoxville, August 2011.

[35] Majdalani, J., "Helical Solutions of the Bidirectional Vortex in a Cylindrical Cyclone: Beltramian and Trkalian Motions," *Fluid Dynamics Research*, Vol. 44, No. 6, October 2012, pp. 065506. doi:10.1088/0169-5983/44/6/065506.

[36] Majdalani, J., "Unified Framework for Modeling Swirl Dominated Helical Motions," *50th AIAA/ASME/SAE/ASEE Joint Propulsion Conference*, AIAA Paper 2014-3677, July 2014. doi:10.2514/6.2014-3677.

[37] Bloor, M. I. G. and Ingham, D. B., "The Flow in Industrial Cyclones," *Journal of Fluid Mechanics*, Vol. 178, No. 1, May 1987, pp. 507–519. doi:10.1017/s0022112087001344.

[38] Barber, T. A. and Majdalani, J., "On the Beltramian Motion of the Bidirectional Vortex in a Conical Cyclone," *Journal of Fluid Mechanics*, Vol. 828, September 2017, pp. 708–732. doi:10.1017/jfm.2017.494.

[39] Majdalani, J., "On the Generalized Beltramian Motion of the Bidirectional Vortex in a Conical Cyclone," *Physics of Fluids*, Vol. 34, No. 3, March 2022, pp. 036604. doi:10.1063/5.0083740.

[40] Majdalani, J. and Williams, L. L., "A Quasi Complex-Lamellar Solution for a Hemispherically Bounded Cyclonic Flowfield," *Physics of Fluids*, Vol. 33, No. 8, August 2021, pp. 083105. doi:10.1063/5.0058647.

[41] Williams, L. L. and Majdalani, J., "An Exact Irrotational Solution for a Hemispherically Bounded Cyclonic Flowfield," *Physics of Fluids*, Vol. 33, No. 6, June 2021, pp. 063608. doi:10.1063/5.0051111.

[42] Williams, L. L. and Majdalani, J., "Exact Beltramian Solutions for Hemispherically Bounded Cyclonic Flowfields," *Physics of Fluids*, Vol. 33, No. 8, 2021, pp. 093601. doi:10.1063/5.0063743.

[43] Gupta, R., Kaulaskar, M. D., Kumar, V., Sripriya, R., Meikap, B. C., and Chakraborty, S., "Studies on the Understanding Mechanism of Air Core and Vortex Formation in a Hydrocyclone," *Chemical Engineering Journal*, Vol. 144, No. 2, 2008, pp. 153–166. doi:10.1016/j.cej.2008.01.010.

[44] Neesse, T. and Dueck, J., "Air Core Formation in the Hydrocyclone," *Minerals Engineering*, Vol. 20, No. 4, April 2007, pp. 349–354. doi:10.1016/j.mineng.2007.01.007.

[45] Sharma, G. and Majdalani, J., "Effects of Nozzle Inlet Size and Curvature on the Flow Development in a Bidirectional Vortex Chamber," *Physics of Fluids*, Vol. 33, No. 9, September 2021, pp. 093607. doi:10.1063/5.0066121.

[46] Culick, F. E. C., "Rotational Axisymmetric Mean Flow and Damping of Acoustic Waves in a Solid Propellant Rocket," *AIAA Journal*, Vol. 4, No. 8, 1966, pp. 1462–1464. doi:10.2514/3.3709.

[47] Leibovich, S., "The Structure of Vortex Breakdown," *Annual Review of Fluid Mechanics*, Vol. 10, No. 1, January 1978, pp. 221–246. doi:10.1146/annurev.fl.10.010178.001253.

[48] Leibovich, S., "Vortex Stability and Breakdown: Survey and Extension," *AIAA Journal*, Vol. 22, No. 9, September 1984, pp. 1192–1206. doi:10.2514/3.8761.

[49] Alekseenko, S. V., Kuibin, P. A., and Okulov, V. L., *Theory of Concentrated Vortices: An Introduction*, Springer, Berlin, Germany, 2007.

[50] Maicke, B. A. and Talamantes, G., "Numerical Investigation of Injection Variation in the Bidirectional Vortex," *AIAA Journal*, Vol. 55, No. 8, June 2017, pp. 2544–2554. doi:10.2514/1.j055807.

[51] Smith, J. L., "An Analysis of the Vortex Flow in the Cyclone Separator," *Journal of Basic Engineering – Transactions of the ASME*, Vol. 84, No. 4, December 1962, pp. 609–616. doi:10.1115/1.3658722.

[52] Majdalani, J. and Chiaverini, M. J., "Characterization of GO2–GH2 Simulations of a Miniature Vortex Combustion Cold-Wall Chamber," *Journal of Propulsion and Power*, Vol. 33, No. 2, March 2017, pp. 387–397. doi:10.2514/1.b36277.